JOURNAL OF MATERIALS SCIENCE 21 (1986) 165–175

Estimation of power-law creep parameters from bend test data

TZE-JER CHUANG
Center for Materials Science, National Bureau of Standards, Gaithersburg, MD 20899, USA

Power-law creep parameters of brittle ceramic materials are commonly deduced from load-point displacement data generated by four-point bend experiments, under the assumption that tensile and compressive behaviours obey the same constitutive law. However, because of microcracking and cavitation, it is now well recognized that this premise may not always be valid. The present paper presents an analysis which takes the differences into account. Governing equations are first derived for the location of the neutral axis of a beam under bending which does not in general pass through the centroid of the cross-section, and for the creep response in terms of both curvature rate and load-point displacement rate as functions of the applied moment and power-law creep parameters. Numerical solutions are obtained for any given set of material constants over a wide range of applied moments. It is shown from the plots of creep response against applied moment on a logarithmic scale that even linear curves over a narrow range of applied moment do not necessarily imply identical stress exponents, and that non-linear curves concave upward signify a profound difference in stress exponent between tension and compression. An example is given of applying the present analysis to a set of load-point displacement data on glass–alumina beam specimens crept at 1100° C. The results show that the conventional method over/underestimates the creep rates in compression/tension by two orders of magnitude, indicating a need for using the more accurate analysis presented here. Several recommendations are offered to improve the estimation of power-law creep parameters from bend test data.

1. Introduction

The present paper is concerned with steady-state creep deformation behaviour of structural ceramics which are candidate materials for high-temperature stress-bearing applications, and aims at developing a mathematical scheme for which individual tensile and compressive power law creep parameters can be estimated from conventional four-point bend test measurements. Instead of directly relying on uniaxial testing, flexural test methods are frequently adopted as an alternative to generate data from which information on materials' creep behaviour may be extracted (see for example [1, 2]). This practice can be attributed to the fact that a bending experiment is more stable and easier to perform without involving problems of fixturing and alignment usually associated with tension testing of brittle materials at high temperatures. A challenging issue that must be resolved for a given set of data produced from crept bend bars is: how can one, if possible, accurately estimate the uniaxial creep behaviour (both in tension and in compression) when the applied stress is given? Since bending data contain both tensile and compressive components, it is perhaps natural to expect that the resulting predictions would be strongly influenced by the form of the constitutive equations assumed *a priori*.

Extensive literature review on the thermal creep of ceramics [3] indicates that generally speaking the steady-state behaviour relating creep strain rate $\dot{\varepsilon}_s$ to applied stress σ can be described by Norton's law in a form $\dot{\varepsilon}_s = A\sigma^n$, where A is a pre-exponent constant depending only on the test temperature and the material's properties; n is a stress exponent which may or may not depend on stress. Hollenberg *et al.* [4] presented the first analysis in which stresses and strains in the crept beam specimens can be calculated from the bend test data, provided the tensile power-law creep behaves identically to its compressive counterpart. This simplifies the analytical work substantially and allows the solutions to be presented in closed forms, as the neutral axis location in this case always coincides with the centre line of the beam height regardless of the magnitude of the applied loads.

However, it is now well recognized that tensile response might be distinct from its compressive counterpart inside a beam for a given material, even when tested under identical environments (see for example [5, 6]). Consequently, for application to plain concrete, Krajcinovic [7] developed a damage theory for beams under pure bending in order to justify that tensile stresses assume a parabolic distribution in terms of strain while the compression behaviour remains linearly elastic obeying Hooke's law. More recently, Rosenfield *et al.* [8] extended this time-independent analysis to two more constitutive equations in tension, namely linear elastic with lower

0022–2461/86 $03.00 + .12

effective Young's modulus and elastic–perfectly plastic while once again leaving the compressive portion unchanged. On the other hand, within the arena of power-law creep, Finnie [9] was the first to recognize the possible situation of pronounced differences between tensile and compressive creep. His analysis permits $A_t \neq A_c$ and is capable of predicting creep rates from data generated by creep bending of a trapezoidal cross-section beam, provided n_t and n_c are equal to unity; here subscripts t and c refer to the cases of tension and compression respectively. Talty and Dirks [10] extended the analysis of the same trapezoidal beam to a more general case of N, an arbitrary number including unity (i.e. $n_t = n_c = N$).

The present paper extends the previous work to a completely general case of unequal tension and compression power-law creep behaviours, wherein not only the pre-exponent factors are permitted to be distinctive ($A_t \neq A_c$) but also the stress exponent constants may be unequal ($n_t \neq n_c$). For the sake of simplicity, only rectangular beams of uniform cross-sections are considered. Further, the existence of a steady-state is assumed so that time can be eliminated as a variable in the study. This assumption requires that the transient stage be short-lived and thus can be ignored, although it should be acknowledged that this phenomenon may sometimes become important [11, 12] when a well-defined steady state does not develop [13].

In the next section, governing equations are first derived which relate separately the position of the neutral axis and the applied moment to the curvature rate, $\dot{K}$ and (unknown, *a priori*) power-law creep parameters. Computer programs were developed to solve these coupled non-linear algebraic equations numerically. Solutions are obtained in graphic form for an arbitrary set of power law constants. Graphic solutions are also given in terms of the load-point displacement rate, $\dot{\Delta}_p$ – a more measurable quantity than $\dot{K}$ for collecting data on a specimen's response. Cases of $n_t = n_c = N$ as examined by Talty and Dirks [10], and $A_t = A_c = A$, $n_t = n_c = N$ as analysed by Hollenberg *et al.* [4] are then presented as special cases of the present investigation. From the point of view of an experimenter, in order to apply the current theory, a parametric study method must be used from which curves can be produced from the computer programs to match the discrete data points which are dictated by creep bend tests. Once accurate matching is achieved,the predicted power-law parameters become available at once from the well-fitted curve. For the sake of demonstration of how to use the theory, an example is given to estimate the four power-law constants from a set of six bend test data on debased alumina beams crept at 1100° C for a duration of more than 100 h. At the conclusion, we are able to make some recommendations from the present analysis for those who prefer using the four-point bend test method to characterize power-law creep behaviour in structural ceramics. These suggestions should lead to more accurate characterization of creep properties.

2. Analysis

2.1. Derivation of the governing equations

In this section, we derive the control equations that relate material response to external variables and material constants, for a rectangular beam under four-point creep bending (Fig. 1).

As already discussed in the preceding section, under the action of some constant external loads the material is assumed to respond in the steady state according to a power law of the form

$$\dot{\varepsilon}_{sc} = A_c(\sigma/\sigma_0)^{n_c} \qquad \sigma \text{ in compression} \qquad (1a)$$

and

$$\dot{\varepsilon}_{st} = A_t(\sigma/\sigma_0)^{n_t} \qquad \sigma \text{ in tension} \qquad (1b)$$

where $\dot{\varepsilon}_s$ is steady-state creep strain rate; A and n are material constants, σ is the normal stress and σ_0 is a reference stress. The subscripts c and t refers to the case in compression and in tension respectively. A schematic sketch of Equation 1 applied to a beam is given in Fig. 2.

The derivation that follows adopts the conventional simple beam theory which entails a fundamental assumption, known as Bernoulli's hypothesis, that planar sections remain plane during bending when creep is taking place so that no warping will occur (because of the need for geometric compatiblity this condition seems to hold in practice [14]). This implies that the strain rate $\dot{\varepsilon}$ of a fibre element is linearly dependent on Y, the distance away from the neutral axis where $\dot{\varepsilon} = 0$, and the curvature rate $\dot{K}$ serves as a proportionality constant. Thus

$$\dot{\varepsilon} = \dot{K}Y$$

and the stress distribution over the cross-section of the beam is highly non-linear and has the following form, according to Equation 1:

$$\sigma(Y) = \sigma_0\left(\frac{Y\dot{K}}{A}\right)^{1/n} \qquad (2)$$

regardless of the sign of the stress. Equilibrium requirements then dictate that the total force acting on the compression side of the cross-section be counter-balanced by its tensile counterpart. This means that $F_c = F_t$ or $B\int_0^{H_c} \sigma \, dY = B\int_0^{H} \sigma \, dY$ where B is the beam width and $H(= H_c + H_t)$ is the beam height (see Fig. 1). By integrating σ using Equation 2 and 1, and after some mathematical manipulations, this force balancing equation finally reduces to

$$\left\{R^{1/(n_t+1)}\dot{k}^{(n_t-n_c)/n_c(n_t+1)} \times \left[\frac{n_c(n_t+1)}{n_t(n_c+1)}\right]^{n_t/(n_t+1)}\right\} \times h_c^{n_t(n_c+1)/n_c(n_t+1)} + h_c = 1 \qquad (3)$$

where $R = A_t/A_c$, $\dot{k} = \dot{K}H/A_c$ and $h_c = H_c/H$ are dimensionless parameters. Here we choose A_c as normalizing factor for R and $\dot{K}$ presumably because A_c is much easier to measure than A_t. Equation 3 is a non-linear algebraic equation of the form $Cx^n + x = 1$ for the unknown h_c quantifying the physical location of the neutral axis. Since both C and n are positive definite, because parameters appearing in Equation 3

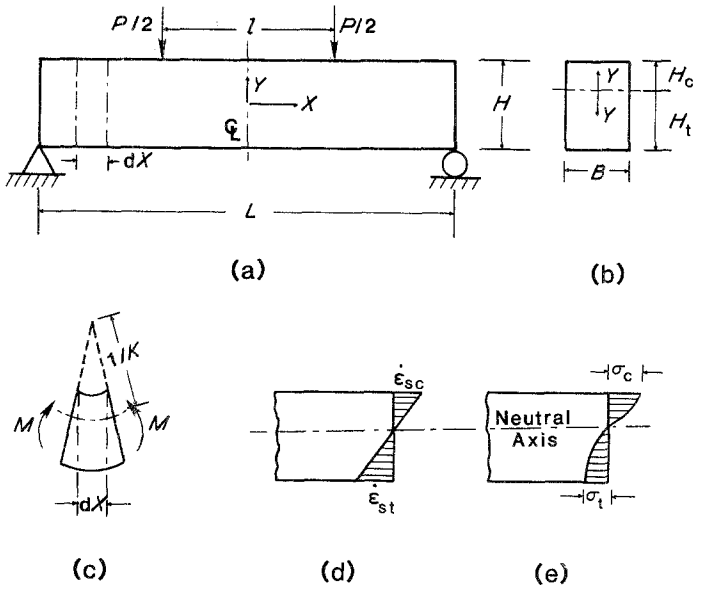

Figure 1 Schematic sketches of a four-point bend beam: (a) loading configuration, (b) representative cross-section, (c) typical element of deformed shape, (d) strain-rate distribution and (e) stress distribution. ℄ denotes centre line of the beam.

are all positive quantities, it can be proved from the form of this non-linear algebraic equation that a unique solution for x always exists in the range $0 < x < 1$ beyond which no physical meaning may be assigned to x.

In addition, the requirement that the total summation of moments produced by local tractions be equated to the external moment M forms the second governing equation, namely

$$M = \int_0^{H_c} + \int_0^{H_t} \sigma Y B \mathrm{d}Y$$

Substitution of Equation 2 for $\sigma = \sigma(Y)$ and recognition of $h_t + h_c = 1$ result in an equation relating the applied moment to the material's response $\hat{k}$:

$$m = \hat{k}^{1/n_c}\left[\frac{\hat{k}^{1/n_t - 1/n_c}}{R^{1/n_t}} \frac{n_t}{2n_t + 1}(1 - h_c)^{(2n_t+1)/n_t} + \frac{n_c}{2n_c + 1} h_c^{(2n_c+1)/n_c}\right] \quad (4)$$

where $m = M/(BH^2\sigma_0)$ is the normalized applied moment. The assignment of the reference stress σ_0 is somewhat arbitrary. Since the unit of the applied stress is generally expressed in MPa, it is convenient to set $\sigma_0 = 1$ MPa for simplicity.

Equations 3 and 4 constitute a system of algebraic equations for the two unknowns h_c and $\hat{k}$, while the remaining parameters such as the applied moment m and the values of the materials parameters A and n are being treated as given. After examining the structure of these two equations, we arrive at the unfortunate conclusion that analytical solutions in closed form cannot be obtained because they are highly non-linear and coupled in $\hat{k}$. Accordingly, a numerical approach is the practical way to tackle this problem. A computer program was developed which contains the following primary tasks: first the development of a subroutine to solve h_c from Equation 3 by a Newton–Raphson iteration scheme. Inputs to this subroutine are R, n_t, n_c and $\hat{k}$, the latter being treated as an independent variable. Note that initially an overshoot outside the range (0,1) for h_c may arise during numerical iterations; stability can then be restored if h_c be reset to its

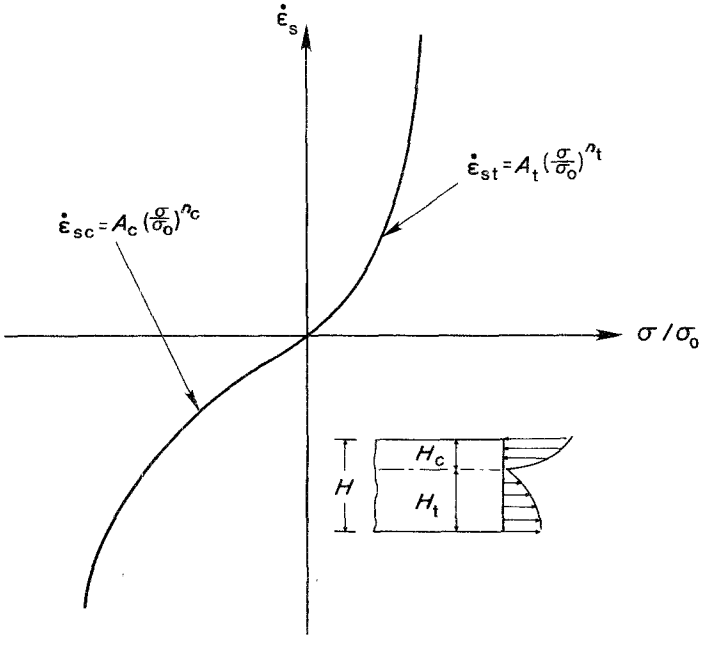

Figure 2 Schematic diagram of power- law constitutive equations in creep, showing distinct behaviours between tension and compression.

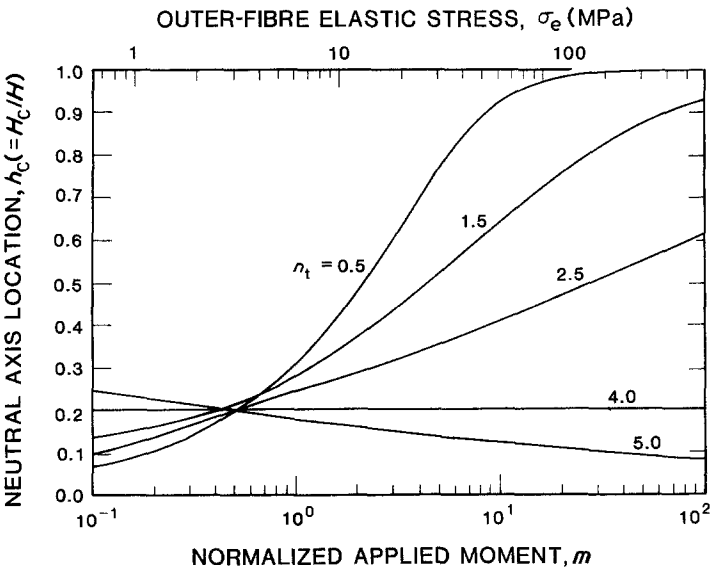

Figure 3 Solutions for normalized compressive size h_c as a function of the applied bending moment m at $n_c = 4$, $R = 1000$ and $n_t = 0.5$, 1.5, 2.5, 4.0 and 5.0.

boundary value. Once h_c is successfully solved from this subroutine it can then be used as input, together with the independent variable $\dot{k}$, to Equation 4 for the computation of m. At the end, a total of three one-dimensional arrays were generated, namely m, $\dot{k}$ and h_c. This concludes the computation phase of programming, and the plotting phase follows. The solutions were then displayed in graphic form for $\dot{k}$ against m as well as h_c against m with any given values of A and n.

2.2. General solutions

2.2.1. Location of neutral axis, h_c

The solutions for h_c are plotted as a function of m in Fig. 3 for several of n_t at $n_c = 4.0$, $R = 1000$. Generally speaking for the practical range of $m > 0.5$, as the applied stress increases the compressive zone keeps shrinking with increasing n_t. Intuitively this must be true since an increase in n_t implies that the material's ability to support tensile stresses is reduced for a fixed creep rate. When $n_t = n_c$, $h_c \approx 0.2$, independent of the applied stress. In fact, h_c can be expressed analytically in the case of equal n. This special case will be discussed later. Another interesting observation that can be extracted from Fig. 3 is at a value of around one half, h_c is about 0.2 regardless of the value of n_t. As a matter of fact, when examined over a broader range we found that when m lies between 0.25 and 0.4 the solutions are quite insensitive to both n_t and n_c, suggesting that this range of m should be avoided in a testing programme that aims to characterize the material's creep parameters. Fig. 4 presents another solution for h_c for five values of R, fixing values of n_t and n_c at 1 and 5 respectively. As expected, the higher the value of R the lower the size of compression zone, as high R implies that the material's creep resistance in tension is reduced at a given strain rate (or applied moment). When m exceeds 10, however, a major portion of the beam is in compression for R values up to 1000. Conversely, setting $n_t = 5$ and $n_c = 1$ demonstrated a reverse trend, as shown in Fig. 5 for the same five values of R. Again, cases of higher R result in a smaller compression zone as expected.

2.2.2. Curvature rate of a beam element, $\dot{k}$

The material's response in the form of curvature rate $\dot{k}$ under creep bending for a given applied moment m is plotted in Fig. 6 on a log–log scale for five values of n_t and fixing $n_c = 4$ and $R = 1000$. Two important observations can be made here: (a) the curves appear linear with, of course, always positive slopes when values of n_t are in the neighbourhood of n_c, but when the gap between the values of n_t and n_c widens the curves become non-linear and concave upward; (b) a "blind point" in the vicinity of $m = 1/2$ is also observed, similar to the solutions of h_c. Fig. 7 demonstrates the solutions of $\dot{k}$ upon variation of R under

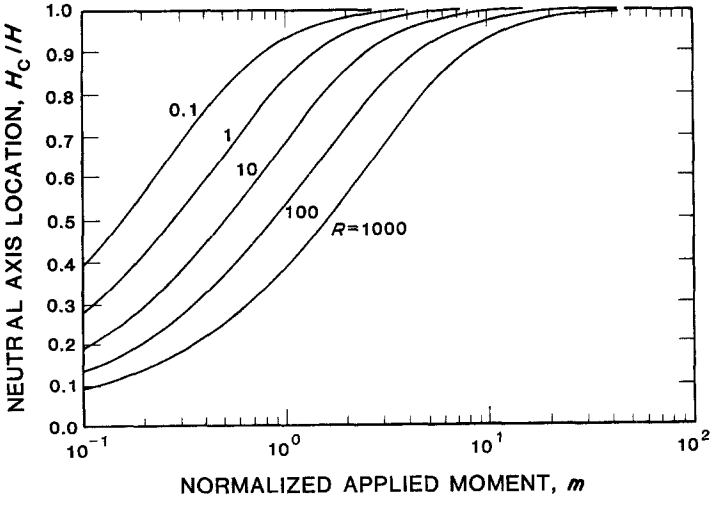

Figure 4 Plots of neutral axis location against the applied moment for $n_t = 1$, $n_c = 5$ and $R = 0.1$, 1, 10, 100 and 1000.

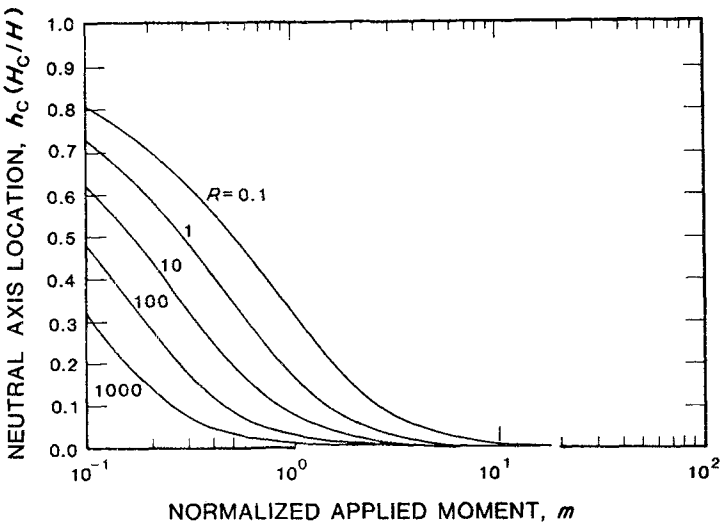

Figure 5 Compressive-zone size solutions as a function of the applied moment at $n_t = 5$, $n_c = 1$ and $R = 0.1$, 1, 10, 100 and 1000.

fixed values of $n_t = 1$ and $n_c = 5$. Again, owing to big differences between the values of n_t and n_c, concave upward curves are obtained. Another interesting feature worthy of note is that the solutions converge into one single straight curve as the applied moment exceeds 15. This means that applying a load in excess of $m = 15$ would generate a straight line in the plot of $\hat{k}$ against m, regardless of the values of R, and therefore this is not particularly useful. Lower loads (much less than $m = 15$) are thus recommended. If, on the other hand, $n_t = 5 \gg n_c = 1$ then the solutions are well-behaved in the practical range of the applied load ($0.01 \leqslant m \leqslant 100$) as indicated in Fig. 8, although most of the solutions appear to be linear.

2.2.3. Outer-fibre stresses, σ_c and σ_t

As can be seen from the preceding section, during steady state creep the neutral axis is displaced from the centroid and the stress distributions are highly nonlinear. As a result, it is to be expected that the outer-fibre stresses, both at the tensile side as well as at the compression side, must in general differ from the initial elastic stress levels. In terms of the applied bending moment M, the outer fibre elastic stresses both in tension and in compression have a value $\sigma_e = 6M/(BH^2)$ from classical simple beam theory, and in terms of dimensionless quantities there results $\hat{\sigma}_e = 6m$, where $\hat{\sigma}_e = \sigma_e/\sigma_0$ is the normalized outer-fibre elastic stress.

The steady-state compressive creep stress at the outer surface of the beam is

$$\sigma_c = \sigma_0(\dot{k}h_c)^{1/n_c}$$

as evidenced from Equation 2. Normalizing against σ_e we have

$$\sigma_c/\sigma_e = \frac{1}{6m}(\dot{k}h_c)^{1/n_c} \tag{5}$$

Similarly the creep stress at the tensile edge, also normalized by σ_e, is

$$\frac{\sigma_t}{\sigma_e} = \frac{1}{6m}[\dot{k}(1 - h_c)/R]^{1/n_t} \tag{6}$$

Examination of these two equations indicates that the outer-fibre creep stresses, unlike their elastic counterparts, are not only a function of applied moment, but also dependent on the neutral axis location and the intrinsic power-law creep parameters. The maximum compressive stresses for several values of n_t are plotted in Fig. 9, according to Equation 5, for typical values of $n_c = 4$ and $R = 1000$. When $m < 0.35$ corresponding to an elastic stress of about 2 MPa, higher values of n_t yield lower compressive stresses; the

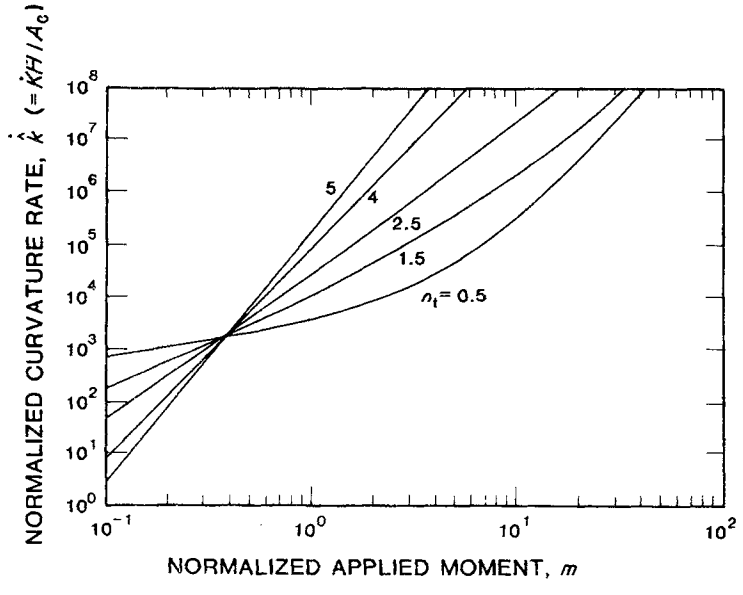

Figure 6 Solutions of normalized curvature rate as a function of applied moment for $n_c = 4$, $R = 1000$ and $n_t = 0.5$, 1.5, 2.5, 4 and 5.

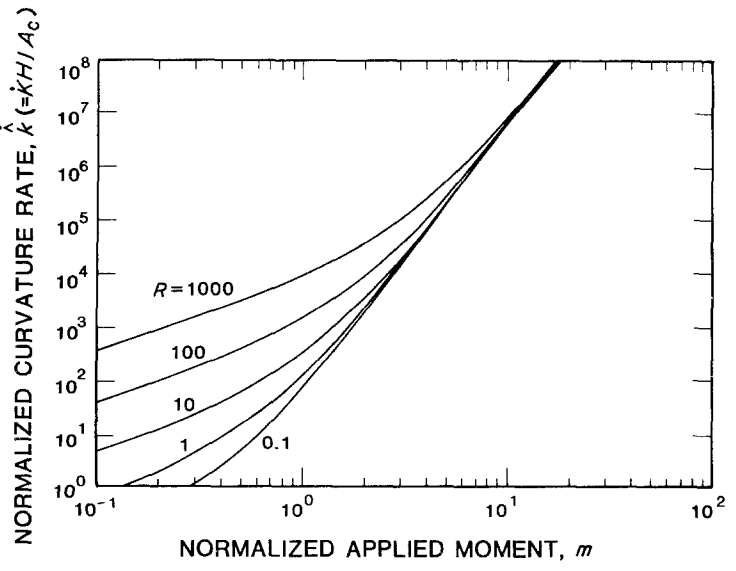

Figure 7 Typical plots of $\dot{\hat{k}}$ against m for $n_t = 1$, $n_c = 5$ and $R = 0.1$, 1.0, 10, 100 and 1000.

reverse situation occurs if the applied stress exceeds 2 MPa. On the other hand the maximum tensile stresses at the outer fibre, as plotted in Fig. 10 from Equation 6, show a unique feature, namely that for a fixed applied load in the practical range (1 to 600 MPa), low values of n_t yield higher tensile creep stresses. Note that in both cases, as shown in Figs. 9 and 10, in the case of $n_c = n_t$ the outer fibre stresses are independent of the applied moment, and as will be shown later in Section 2.3 they can be expressed in closed forms.

2.2.4. Load-point displacement rate, $\dot{\Delta}_p$

As demonstrated in the preceding sections, $\dot{\hat{k}}$ is a proper parameter to measure the response of creep for a bend bar under constant applied moments. Unfortunately, the curvature time-rate of a beam at a fixed location is difficult to measure in the laboratory, and it is general practice to measure instead the load-point displacements continuously as a function of time. Hence, it is desirable to present solutions in terms of $\dot{\Delta}_p$.

For a given material with a well defined $\dot{\hat{k}}$ against m relationship the load-point displacement rate $\dot{\Delta}_p$ incurred from a four-point bend beam can be solved numerically by integration of $\dot{\hat{k}}$ along the beam length x, with linear moment distribution in the outer span and a constant maximum moment in the inner span. Here it is assumed that shear effects on the beam deflection y are negligible and the slopes of the deformed beam shape are small ($dy/dx \ll 1$). The differential equation that needs to be solved is then $d^2\dot{y}/dx^2 = \dot{\hat{k}}(x) = f(m)$ with $\dot{\hat{k}} = f(m)$ given in Section 2.2.2. Setting the origin of the coordinate system at the mid-span of the deformed beam, the proper boundary conditions are $y(0) = 0$ and $y'(0) = 0$ due to symmetry. After the deformed shapes $\dot{y} = \dot{y}(x)$ are solved, the load-point displacement rate is given by $\dot{\Delta}_p = \dot{\Delta}(L/2) - \dot{\Delta}(l/2)$ where L and l are the lengths of major and minor spans respectively. Typical solutions are plotted in Fig. 11 for a non-dimensional load-point displacement rate, defined as $\dot{\Delta}_p/HA_c$ as a function of the applied moment m for several values of n_t with $n_c = 4$, $R = 1000$, $L = 4l$ and $H/l = 1/2$. Similarities between Fig. 6 and 11 are observed. Whenever $n_c = n_t = N$, the solution can be described by a linear curve owing to the fact that the relationship between $\dot{K}_p$ and $\dot{\Delta}_p$ is linear and has a form

$$\dot{K}_p = \frac{4(N+2)}{(L-l)[L+(N+1)l]}\dot{\Delta}_p$$

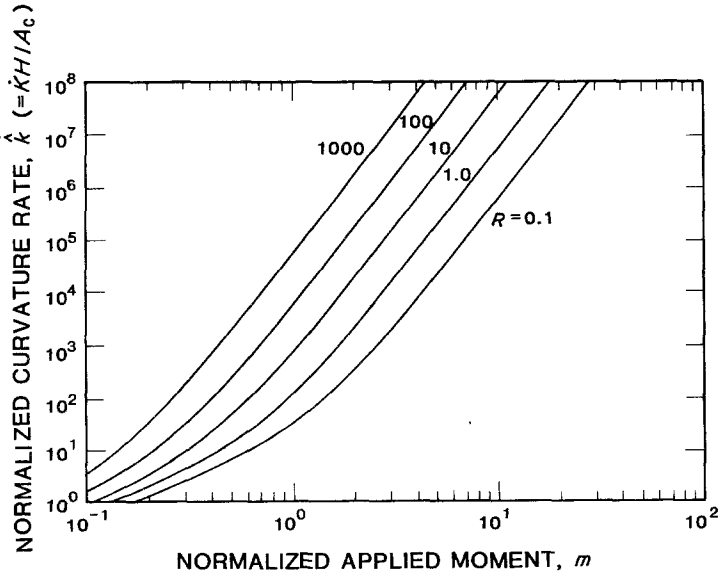

Figure 8 Similar plot to Fig. 7 except $n_t = 5$ and $n_c = 1$.

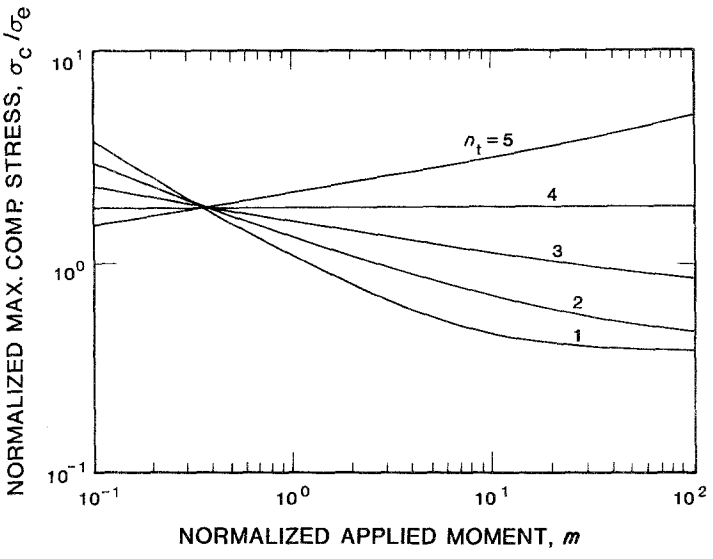

Figure 9 Plots of outer-fibre compressive creep stress normalized against elastic stress against applied moment for $n_c = 4$, $R = 1000$ and $n_t = 1, 2, 3, 4$ and 5.

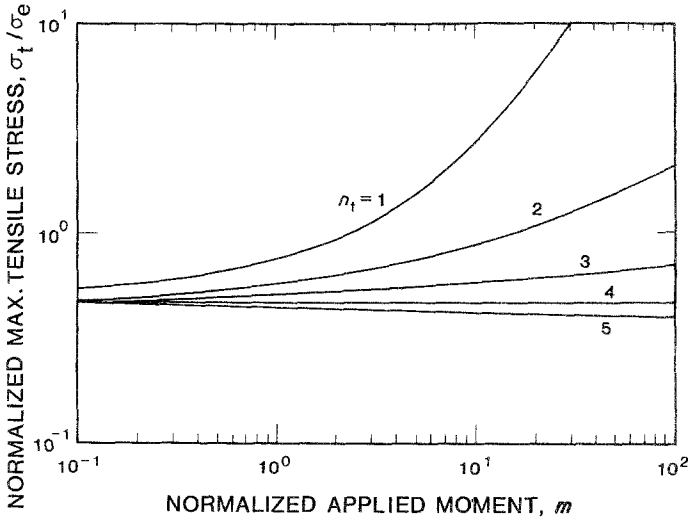

Figure 10 Numerical solutions for normalized outer-fibre tensile stress, (σ_t/σ_e), as a function of m. The material's constants are the same as in Fig. 9.

2.3. The special cases

Having obtained the general solutions in the previous section, it is easy to arrive at the results for the special cases as considered by Hollenberg *et al.* [4] and Talty and Dirks [10].

2.3.1. The case $n_t = n_c = N$; $R \neq 1$

This is the case considered by Talty and Dirks [10] and Cohrt *et al.* [12]. For this case, Equation 3 describing the location of the neutral axis takes the following simple form:

$$h_c = \frac{1}{1 + R^{1/(N+1)}} \tag{7}$$

independent of the applied moment m. This is in agreement with the work of Cohrt *et al.* [12] (See

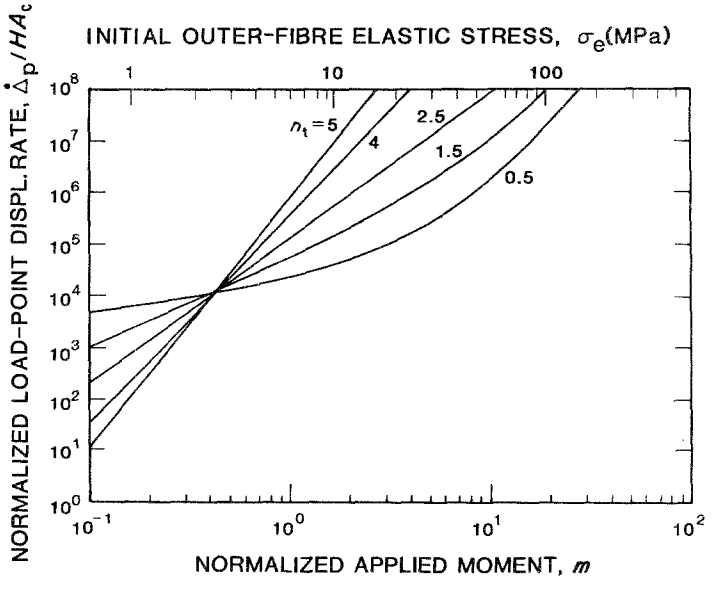

Figure 11 Plots of load-point displacement rate against m for several values of n_t at $n_c = 4$ and $R = 1000$; $H/l = 1/2$ and $L/l = 4$.

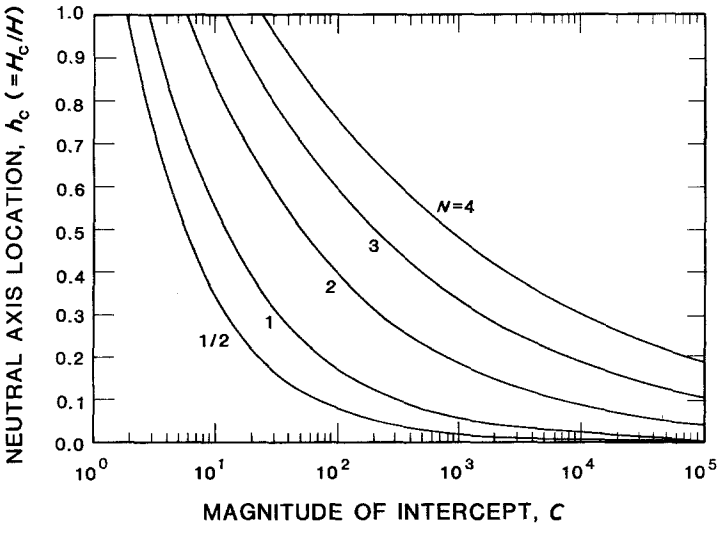

Figure 12 Plots of h_c against C, C being the intercept of the linear plots of $\dot{k}$ against m at $m = 1$; it is thus a measureable parameter. $n_t = n_c = N$.

Equation 3 of [12] in which our R is equivalent to their S^n). In addition, it can be shown from Equation 4 that the moment against curvature rate is linear when plotted on logarithmic scales, and therefore can be described by

$$\dot{k} = Cm^N \tag{8}$$

where C is the intercept at $m = 1$ and is only a function of h_c, R and N:

$$C = \left[\frac{(2N+1)/N}{h_c^{(2N+1)/N} + (1-h_c)^{(2N+1)/N} R^{1/N}}\right]^N \tag{9}$$

Fig. 12 presents the solutions of h_c for several values of N, based on Equation 7 as a function of C defined in Equation 9. Fig. 13 demonstrates the solutions for R. If $n_c = n_t = N$, the bend test data in terms of $\dot{k}$ against m ought to be fitted by a linear curve on a logarithmic axis. A_c is automatically obtainable from $\dot{k}$ and $\dot{K}$ (see Fig. 1 and definition of $\dot{k}$). C as well as N can then be extracted from this curve. Figs. 12 and 13 can then be used to obtain h_c and R (and hence A_t) and the complete creep parameters are determined.

2.3.2. The case of uniform property ($n_t = n_c = N$; $R = 1$)

This case has already been considered by Hollenberg *et al.* [4]. The neutral axis in this case always coincides with the centroid (i.e. $h_c = 1/2$) as can be shown from Equation 7 when $R = 1$ is substituted. Constitutive Equation 8 describing the relations between $\dot{k}$ and m is of course still valid, but the intercept C now takes the simple form

$$C(N) = 2\left(\frac{2N+1}{N/2}\right)^N \tag{10}$$

Fig. 14 is a plot of N against C from Equation 10. This can be used as a first step to check whether the material has uniform properties in creep, by checking the observed value of C to see if it agrees with the predicted value of C given by this plot.

2.4. Application to glass–alumina

As an example of demonstrating the applicability of the present analysis, three loads of different magnitude were applied to beams of debased alumina (commercially known as AD–86* from Coors Corp.) at 1100° C in a four-point bend configuration with major and minor spans set at 40 and 10 mm respectively. Load-point displacements are continuously monitored as a function of time. An apparent steady state was observed in all cases within 40 h. Table I lists the pertinent data of measurements. After data were taken, the first step is to plot $\dot{\Delta}_p$ against m on logarithmic scales. If the resulting curves are linear, the

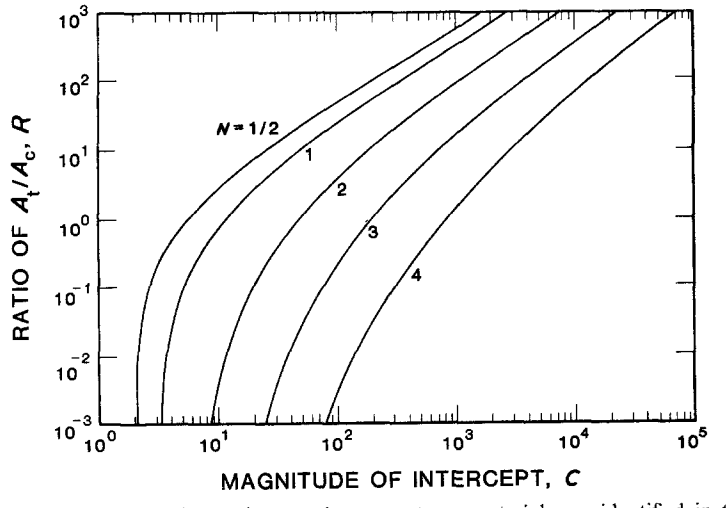

Figure 13 Plots of R against C for the same fixed value of N.

*Certain commercial equipment, instruments or materials are identified in this paper in order to adequately specify the experimental procedure. Such identification does not imply recommendation or endorsement by the National Bureau of Standards, nor does it imply that the materials identified are necessarily the best available for the purpose.

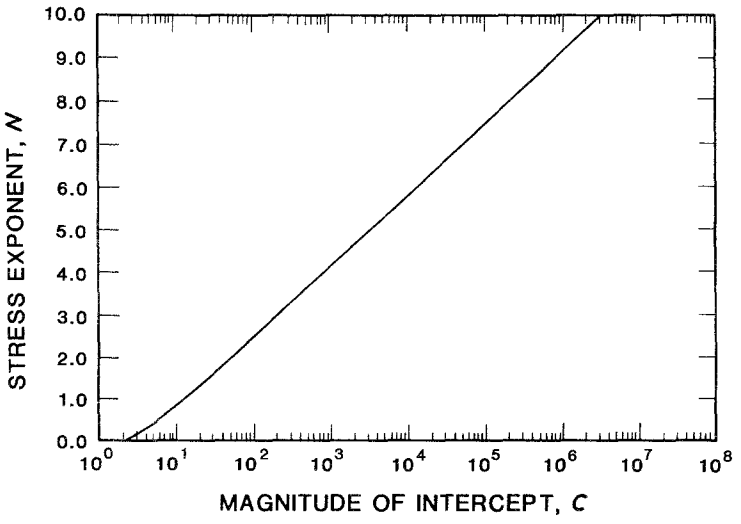

Figure 14 Plots of N against C when $R = 1$ and $n_t = n_c = N$. $\dot{k} = Cm^N$, $C(N) = 2[2(2N + 1)/N]^N$.

solutions presented in Section 2.3 can be used to check whether special cases apply. Since plotting of data in Table I indicated non-linear behaviour (suggesting $n_t \neq n_c$), the special case discussed in Section 2.3 must be ruled out. Solutions of different R and n were produced in order to fit the data points. It was finally found that a special curve as shown in Fig. 15, with constant $n_c = 4$, $n_t = -1/2$ and $R = 50\,000$, fits the data well. A_c was determined from the solution to be $0.85 \times 10^{-13}\,\text{sec}^{-1}$. Thus the steady-state tension creep behaviour of this refractory material can be described by

$$\dot{\varepsilon}_{st} = 4.25 \times 10^{-9}\sigma^{1/2}$$

and the compression creep, on the other hand, by

$$\dot{\varepsilon}_{sc} = 0.885 \times 10^{-13}\sigma^4$$

where $\dot{\varepsilon}$ and σ have the units of sec^{-1} and MPa respectively.

The predications strongly suggest a profound difference of creep behaviour between tension and compression. Uniaxial tension tests were also performed which yield the same order of magnitude as predicted by the current analysis. Additional tests in simple tension as well as in compression are being performed in order to verify the predictions. Detailed microstructures of these post-crept beam specimens are also being investigated in order to understand the rheology leading to the resulting power-law stress exponents. One dominating factor obtained from the preliminary studies is the observation of compositional changes due to devitrification, resulting in drastic variation of viscosity in the grain-boundary liquid phases [15, 16]. This strong stress-dependent viscosity, coupled with local recrystallization in the compression zone and dilatancy and/or cavitation in the tension region, may be responsible for the unequal stress exponents.

In contrast, the conventional method assumes $R = 1$ and $n_t = n_c = N$ so that the outer fibre creep rate can be computed from the load-point displacement rate data by the following equation:

$$\dot{\varepsilon}_{ss} = \frac{2(N + 2)H\dot{\Delta}_p}{(L - l)[L + (N + 1)l]}$$

and the outer-fibre stresses by

$$\sigma = \sigma_e\left(\frac{2N + 1}{3N}\right)$$

Table II lists the resulting outer-fibre creep rates and stresses computed from the same set of load-point displacement data tabulated in Table I. A plot of $\dot{\varepsilon}_{ss}$ against σ_e on logarithmic scales by the least squares method, as shown in Fig. 15, leads to a prediction of $A = 1.71 \times 10^{-11}\,\text{sec}^{-1}$ and $N = 1.86$. Hence we see that there are substantial differences in the prediction of power-law creep parameters between the present analysis and the conventional method. Notice that $A_t < A < A_c$ and $n_t < N < n_c$, implying that the conventional techniques, by imposing uniform properties, effectively generate an average in bending creep.

3. Discussion

We have presented a viable technique by which individual tension and compression creep behaviours, being equal or not, can be predicted directly from bend test data. Several main features in the analysis are noteworthy:

1. The neutral axis of the beam cross-section is, in

TABLE I Calculations of normalized load-point displacement rates from four-point bend data of glass–alumina tested at 1100° C. Power-law creep parameters were then obtained based on the present analysis.

Specimen No.	Beam height H (mm)	σ_e (MPa)	m	$10^{10} \times \dot{\Delta}_p$ (m sec^{-1})	$10^7 \times \dot{\Delta}_p/H$ (sec^{-1})	$10^{-6}\dot{\Delta}_p/HA_c$
1	2.785	20	3.333	5.185	1.862	2.191
2	2.785	20	3.333	4.719	2.694	1.993
3	2.770	30	5.000	6.311	2.278	2.680
4	2.770	30	5.000	6.656	2.403	2.827
5	2.770	40	6.666	11.50	4.152	4.885
6	2.770	40	6.666	11.57	4.177	4.914

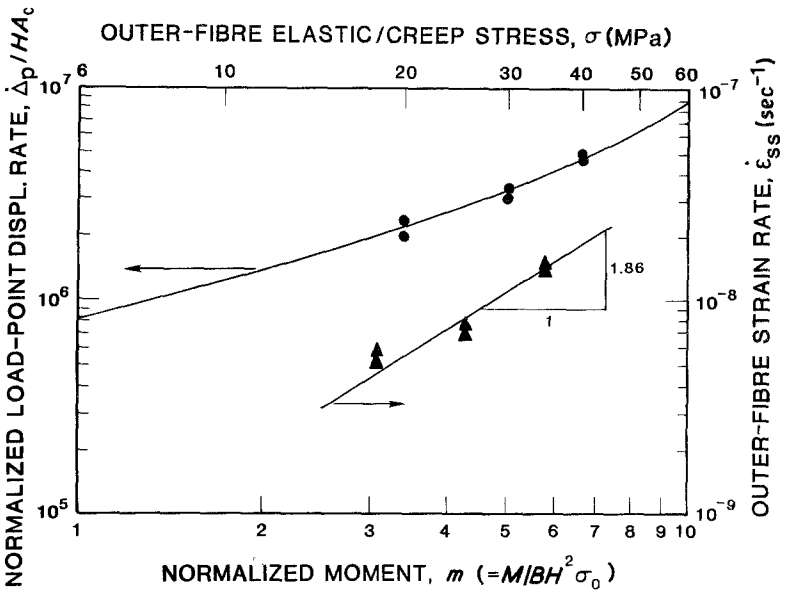

Figure 15 Plot of four-point bend test data on glass–alumina crept at 1100° C in the space of $\log(\dot{\Delta}_p/HA_c)$ against $\log m$, indicating a good match at a solution (●) for $R = 50\,000$, $n_c = 4$ and $n_c = 1/2$. The power-law creep parameters are then predicted as $A_c = 0.85 \times 10^{-13}\,\text{sec}^{-1}$, $n_c = 4$; $A_t = 4.25 \times 10^{-9}\,\text{sec}^{-1}$, $n_t = 1/2$. For comparison purposes, a linear plot based on the conventional method is also given (▲); this predicts $\dot{\varepsilon}_{ss} = 1.71 \times 10^{-11}\sigma^{1.86}$.

general, not located at the centroid; the location is not only a function of the material's constants but also of the applied loads. This is generally indicated by observations of significant densities of cavities developed over 50% of the beam cross-section, suggesting that the neutral axis has migrated towards the compressive side.

2. If a plot of data for $\dot{k}$ against m shows strong non-linearity which is concave upward, there will be a big difference between n_c and n_t.

3. There exists an applied load for all materials, in the neighbourhood of 1 to 2 MPa of initial outer-fibre elastic stress, under which the material response in $\dot{K}$ or $\dot{\Delta}_p$ will be insensitive to n, suggesting that this load level is not useful in the test programme.

4. If $\dot{k}$ against m data demonstrate a linear response on logarithmic axes, then the results given in Section 2.3 can first be used to ascertain whether the material possesses uniform creep properties. Otherwise, the general solution scheme as detailed in Section 2.1 has to be adopted since a linear curve within a short range of m does not necessarily mean that $n_t = n_c$ as evidenced from Fig. 7. An example was given in Section 2 to show how to apply the current analysis to a realistic case.

However, the analysis does have some restrictions and limitations built in which ought to be borne in mind. First, the constitutive law is assumed to take a power-law equation form with the distinction being made through the variations in n and A. Microscopic observations including scanning electron microscopy (SEM and STEM) have showed that in a general ceramic system, cracks and cavities are developed in different patterns both in terms of density and orientations inside the tensile and compressive zones of a crept bend specimen. Hence, cracking and cavitation play an important role in the contribution to creep resulting in distinct behaviours. Secondly, no deformation mechanism changes are assumed to take place under uniaxial loading so that a single power-law equation completely characterizes the creep behaviour. Consequently, the current analysis is not applicable to materials exhibiting bi-linear law, although in principle a numerical scheme may be developed to handle this case. Finally, the problem of creep fracture is not addressed in this paper. As a result, the solutions presented here are assumed to be valid irrespective of how high a load is applied. Realistically, however, as the loads become higher and higher, the solutions will always be termed invalid somewhere by premature failure due to void growth and flaw linkage. The prediction of rupture time as a function of applied stress is thus an important area which warrants further studies.

Rosenfield *et al.* [8] recently presented a similar time-independent analysis on a beam with three different tensile laws. By fixing the compression behaviour as linearly elastic, they found an interesting result that at 1/5 of the beam depth from the tension

TABLE II Computation of strain rates for the same set of data listed in Table I. Different power-law creep parameters were then predicted based on conventional method.

Specimen No.	Beam height H(mm)	Outer-fibre elastic stresses σ_e(MPa)	Outer-fibre creep stresses σ(MPa)	$10^{10} \times \dot{\Delta}_p$ (m sec^{-1})	$10^9 \times$ creep rate $\dot{\varepsilon}_{ss}$(sec^{-1})
1	2.785	20	16.93	5.185	5.417
2	2.785	20	16.93	4.719	4.930
3	2.770	30	25.40	6.311	6.557
4	2.770	30	25.40	6.656	6.916
5	2.770	40	33.87	11.50	11.951
6	2.770	40	33.87	11.57	12.020

Note: $\sigma = \left(\frac{2N+1}{3N}\right)\sigma_e$, $\dot{\varepsilon}_{ss} = \frac{2(N+2)H\dot{\Delta}_p}{(L-l)[L+(N+1)l]}$; $N = 1.86$, $L = 40$ mm, $l = 10$ mm.

edge, the stress there is fairly fixed regardless of the form of the tensile deformation law. However, with the removal of the assumption of linear behaviour in compression, the results given by the present analysis did not show this feature. Accordingly, we must conclude that their results possess a strong limitation induced by the imposed linear elastic behaviour in compression.

4. Summary and recommendations

In lieu of a summary of the analysis presented in the paper, the following recommendations are offered to experimenters who intend to use bend tests for characterizing a material's creep behaviour:

1. The range of the applied loads should be as wide as possible; at least two orders of magnitude in loads (e.g. 5 to 600 MPa) are recommended.

2. In the case where higher moments cannot be achieved owing to premature fracture, a supplemental test programme either in tension or in comparison should be performed for the purpose of reducing computer work, thus improving the accuracy of the results.

3. Direct measurements of uniform curvature rate in the inner span are preferred to load-point displacements measurements, as the latter induce complications such as shearing effects, although the former may be more difficult to do.

Acknowledgements

Financial support by the AR&TD Fossil Energy Materials programme of the US Department of Energy under Interagency Agreement DE–A105–800R20679 and by the US Air Force Office of Scientific Research under Agreement AFOSR–ISSA–84–00013 with NBS are hereby acknowledged. The author is grateful to Professor Karl Jakus of the University of Massachusetts, Amherst, Massachusetts for carrying out the bending experiment on glass-bonded alumina, and to Drs Richard J. Fields and Sheldon M. Wiederhorn of the National Bureau of Standards for critically reviewing the manuscript.

References

1. S. U. DIN and P. S. NICHOLSON, *J. Mater. Sci.* **10** (1975) 1375.
2. *Idem, J. Amer. Ceram. Soc.* **58** (1975) 500.
3. W. R. CANNON and T. G. LANGDON, *J. Mater. Sci.* **18** (1983) 1.
4. G. W. HOLLENBERG, G. R. TERWILLIGER and R. S. GORDON, *J. Amer. Ceram. Soc.* **54** (1971) 196.
5. M. S. SELTZER, *Bull. Amer. Ceram. Soc.* **56** (1977) 418.
6. R. MORRELL and K. H. G. ASHBEE, *J. Mater. Sci.* **8** (1973) 1253.
7. D. KRAJCINOVIC, *J. Appl. Mech.* **46** (1979) 592.
8. A. R. ROSENFIELD, D. K. SHETTY and W. H. DUCKWORTH, *J. Mater. Sci.* **20** (1985) 935.
9. I. FINNIE, *J. Amer. Ceram. Soc.* **49** (1966) 218.
10. P. K. TALTY and R. A. DIRKS, *J. Mater. Sci.* **13** (1978) 580.
11. T. FETT and D. MUNZ, *ibid.* **19** (1984) 1791.
12. H. COHRT, G. GRATHWOHL and F. THGUMMLER, *Res. Mechanica* **10** (1984) 55.
13. R. M. ARONS and J. K. TIEN, *J. Mater. Sci.* **15** (1980) 2046.
14. G. H. MacCULLOUGH, *Trans. ASME (Appl. Mech.)* **1** (1933) 55.
15. S. M. WIEDERHORN, B. J. HOCKEY, R. F. KRAUSE and K. JAKUS, *J. Mater. Sci.*, in press.
16. W. D. KINGERY, H. K. BOWEN and D. R. UHLMANN, "Introduction to Ceramics" (Wiley, New York, 1976) p. 757.

Received 23 November 1984
and accepted 28 February 1985